Morphofunctional changes at the active zone during synaptic vesicle exocytosis

This manuscript (permalink) was automatically generated from aseedb/synaptic_tomo_ms@ba83ebd on August 31, 2021.

Authors

- **Julika Radecke**[*]
  0000-0002-5815-5537 · julikaradecke
  Institute of Anatomy, University of Bern, Bern, Switzerland; Department of Neuroscience, Faculty of Health and Medical Sciences, 2200 Copenhagen N, University of Copenhagen, Copenhagen, Denmark; Diamond Light Source Ltd, Didcot, Oxfordshire, United Kingdom · Funded by Grant XXXXXXXX

- **Raphaela Seeger**[*]
  XXXX-XXXX-XXXX-XXXX · elatella
  Institute of Anatomy, University of Bern, Bern, Switzerland; Graduate School for Cellular and Biomedical Sciences, University of Bern

- **Anna Kádková**

  Department of Neuroscience, University of Copenhagen, Blegdamsvej 3B, 2200 Copenhagen N, Denmark

- **Ulrike Laugks**
  0000-0003-4175-4354
  Max-Planck-Institute of Biochemistry, Am Klopferspitz 18, 82152 Martinsried, Germany

- **Kenneth N. Goldie**
  0000-0002-7405-0049
  Center for Cellular Imaging and NanoAnalytics, Biozentrum, University of Basel, Basel, Switzerland

- **Henning Stahlberg**
  0000-0002-1185-4592 · sthennin
  Center for Cellular Imaging and NanoAnalytics, Biozentrum, University of Basel, Basel, Switzerland; EPFL; UNIL

- **Vladan Lučić**
  0000-0003-3698-7436 · vladanl
  Max-Planck-Institute of Biochemistry, Am Klopferspitz 18, 82152 Martinsried, Germany

- **Jakob B. Sørensen**[✉]
  0000-0001-5465-3769 · JBSorensen
  Department of Neuroscience, University of Copenhagen, Blegdamsvej 3B, 2200 Copenhagen N, Denmark · Funded by Novo Nordisk Fonden, NNF17OC0028516.; Carlsbergfondet, CF17-0875; Independent Research Fond Denmark, 8020-00228A; Lundbeckfonden, R277-2018-802

- **Benoît Zuber**[✉]
  0000-0001-7725-5579 · aseedb
  Institute of Anatomy, University of Bern, Bern, Switzerland · Funded by Swiss National Science Foundation, 179520; ERA-NET NEURON, NEURON-119

✉ Address correspondence to benoit.zuber@ana.unibe.ch and jakobbs@sund.ku.dk.

* These authors contributed equally.

Abstract

The fusion of synaptic vesicles (SVs) with the plasma membrane (PM) proceeds through intermediate steps that remain poorly resolved. Additionally, the effect of persistent high or low exocytosis activity on intermediate steps remains unknown. Through time-resolved cryo-electron tomography, we ordered events into a sequence. Following stimulation, additional SVs are rapidly primed by forming tethers with the PM. Simultaneously, fusion initiation occurs by membrane curvature ('buckling') of the SV and PM. It is followed by the formation of a fusion pore, and the collapse of SV membrane. At this time, membrane-proximal, but not membrane-distal, vesicles lose their interconnections, allowing them to move towards the PM. Two mutations of SNAP-25 that arrests or disinhibit spontaneous release, respectively, both caused a loss of interconnectors, while the disinhibiting mutant also caused a loss of membrane proximal multiple-tethered SVs. Overall, tether formation and connector dissolution is triggered by stimulation and respond to the spontaneous fusion rate. These morphological observations likely correspond to the transition of SVs from one functional pool to another.

Introduction

In the central nervous system, neurons communicate through the release of neurotransmitters at synapses. This process relies on synaptic vesicle (SV) exocytosis, i.e. the fusion of SVs with the plasma membrane (PM). This in turn is eminently important for normal brain function such as movement coordination or memory formation. SV exocytosis involves a sequence of steps [1,2]. The vesicle is docked to the active zone (AZ) PM and the exocytosis machinery goes through a maturation process, termed priming, after which the SV is ready to fuse. These SVs form the readily releasable pool (RRP) of SVs. Finally, a calcium influx triggers fusion of the SV with the PM. Docked SVs are defined as the SVs in very close proximity or direct contact with the PM as observed by electron microscopy (EM), whereas priming refers to SV ability to undergo exocytosis immediately upon stimulation. Whether every docked SV is also primed has been debated [1,3,4]. A high-pressure freezing/freeze-substitution EM study of genetically modified synapses has indicated that vesicles that are in direct contact with the PM, i.e. docked, are also primed and belong to the RRP and that this situation occurs downstream of vesicle tethering [4]. From a molecular perspective, priming involves several proteins, including the SNARE complex (SNAP-25, syntaxin-1, and synaptobrevin-2), Munc13, Munc18, synaptotagmin-1, and complexin [2,5]. All three SNAREs form a highly stable tight four-helix bundle, known as trans-SNARE complex. The surfaces of the SV and the PM, respectively, are negatively charged and therefore tend to repulse each other. The formation of the trans-SNARE complex counteracts this repulsion and brings the SV and the PM in high proximity [6]. Evidence has suggested that the SNARE complex is only partially zipped in primed SVs [7]. Furthermore, various studies have suggested that the formation of at least three SNARE complexes provides the necessary energy for a SV to become fusion-competent [8,9,10]. Yet in the absence of cytoplasmic Ca^{2+}, minimal spontaneous exocytosis takes place. When the presynaptic terminal gets depolarized by an action potential, Ca^{2+} flows in the cytoplasm and binds to synaptotagmin-1, which is localized at the SV surface. Upon Ca^{2+} binding, synaptotagmin-1 was proposed to insert between the head groups of the PM anionic phospholipids and trigger membrane curvature and destabilization, leading first to hemifusion and subsequently to fusion[11]. Interestingly, much of the trans-SNARE bundle surface is negatively charged, which contributes to the electrostatic barrier that minimizes spontaneous fusion and allows synaptotagmin-1 to act as an electrostatic switch that triggers exocytosis [12]. Introducing negatively charged side chains by site-directed mutagenesis reduces the rate of spontaneous and evoked exocytosis whereas introducing more positive side chains enhances the rate of spontaneous exocytosis and depletes the RRP.

Cryo-electron tomography (cryo-ET), which preserves samples to atomic resolution, revealed that under resting conditions, no SV is in direct contact with the PM and the majority of AZ-proximal SVs are connected to the PM by a variable number of short tethers [13,14]. The observed gap between the SV and the PM is consistent with the model of an electrostatic barrier formed by the negative charges of the SV, the PM, and the trans-SNARE bundle [12]. In synaptosomes treated with hypertonic sucrose solution, which depletes the RRP, the majority of tethered vesicles had only 1 or 2 tethers [13,15,16]. This observation suggested that the RRP consists of SV that are linked to the PM by 3 or more tethers. The RRP, as identified by morphological criteria, only represents a minority of AZ-proximal vesicles. This is in agreement with previous reports. In one of them the term pre-primed pool was used for the few vesicles (~1 vesicle at hippocampal synapses) that are rapidly released and another publication showed that the immediately releasable pool is made up of only 10-20% of the vesicles located on the AZ (equal to ~1 vesicle on hippocampal synapses) [17,18]. The ensemble of proximal vesicles that are not in the RRP have been termed non-RRP and presumably belong to the recycling pool that releases more slowly [13,19]. Farther away from the AZ, partially intermixed with the recycling pool, is the reserve pool containing vesicles that only release upon high frequency stimulation. Vesicles in the reserve pool are tightly clustered and well inter-connected by structures that were termed connectors [13,19]. It should be noted that the molecular nature of connectors is not known and is possibly heterogenous. Synapsin has been proposed as a molecular constituent but since the deletion of all forms of synapsin does not lead to the complete absence of connectors, it is clear that not all connectors contain synapsin [20,21]. The second row of SVs near the active zone, immediately after the proximal vesicles, is called the intermediate region. Resting state intermediate SVs are less densely packed and also less connected than proximal SVs [14]. This suggests that, after exocytosis of RRP SVs, intermediate SVs could be rapidly recruited in the RRP by diffusion [22]. Synaptic activity enhances the mobility of a fraction of SVs, whereas it induces synapsin dissociation from SVs in a synapsin phosphorylation-dependent manner [23,24]. The same mobility enhancement can be achieved through inhibition of synapsin dephosphorylation, which leads to synapsin dissociation from SVs, or by knocking out all three synapsin forms [25,26,27]. Interestingly, ribbon synapses do not express synapsin and show higher SV mobility than conventional synapses [28]. It is therefore conceivable that inter-SV connectors restrain SV diffusion and that synaptic activity influences the level of inter-SV connectivity and thereby their mobility.

To investigate this hypothesis and to better understand the impact of depolarization and synaptic activity on SV tethering, we designed two sets of cyro-ET experiments. On the one hand, we compared the morphology of wild-type rat synaptosome in resting state and a few milliseconds after depolarization. On the other hand, to study the consequences of increased or decreased spontaneous synaptic activity, we imaged synapses in mice neuronal culture expressing either wild-type SNAP-25, a more positively charged SNAP-25 mutant (4K mutant), or a more negatively charged mutant of SNAP-25 (4E mutant). The more positive SNAP-25 mutant, which is constitutively active showed no triple-tethered SV, which confirmed the morphological definition of the RRP. Our experiments revealed that immediately after depolarization additional SVs are recruited to the RRP. Shortly after exocytosis the level of inter-SV connectivity was decreased among SVs situated in a 25 to 75-nm distance range from the AZ PM. Altogether, our results indicate that connectors regulate SV mobility and their recruitment at the AZ PM.

Results

To analyze the morphological changes occuring in the presynpase shortly after stimulation, we pursued a time-resolved cryo-electron tomography approach. A 52-mM KCl containing buffer was sprayed with an atomizer to depolarize synaptosomes and stimulate exocytosis milliseconds before vitrification. The spray droplet size was optimized by cutting a 1-ml pipet tip to a diameter matching an EM grid (3 mm) and fixed to the atomizer glass outlet to disperse the spray (Figure 1A1). Furthermore, to achieve a delay of 7 ms between spraying and freezing, the nozzle was set 1-2 mm above the liquid ethane container. This generated many small spray droplets spread throughout the

grid (Figure 1A2-A4). Even if sprayed droplets were well distributed throughout the grid, not all synaptosomes were in contact with exocytosis-triggering KCl solution. Given the very low throughput of cryo-electron tomography, we followed a correlative light and electron microscopy approach. By cryo-fluorescence microscopy, we identified areas where fluorescently labeled synaptosomes and fluorescent spray droplets were colocalized. Additionally, phase contrast imaging enabled quality control of the frozen EM grid with respect to ice contamination and ice cracks, as shown previously [29]. 9 control and 9 stimulated synaptosome tomograms were analyzed. We restricted our analysis to synaptosomes that possessed a smooth PM, free of signs of rupturing and that had a mitochondrion, as we considered these factors essential for synaptosome function.

In addition, we manipulated the electrostatic state of the SNARE complex through a series of point mutations introduced above and grew primary neurons on EM grids [12] (Figure 1B1-B4). ***More text from Julika and Jakob to describe the procedure here***. Thereby we could image chronically overactive or depressed synapses and relate presynaptic architectural modifications to different functional states.

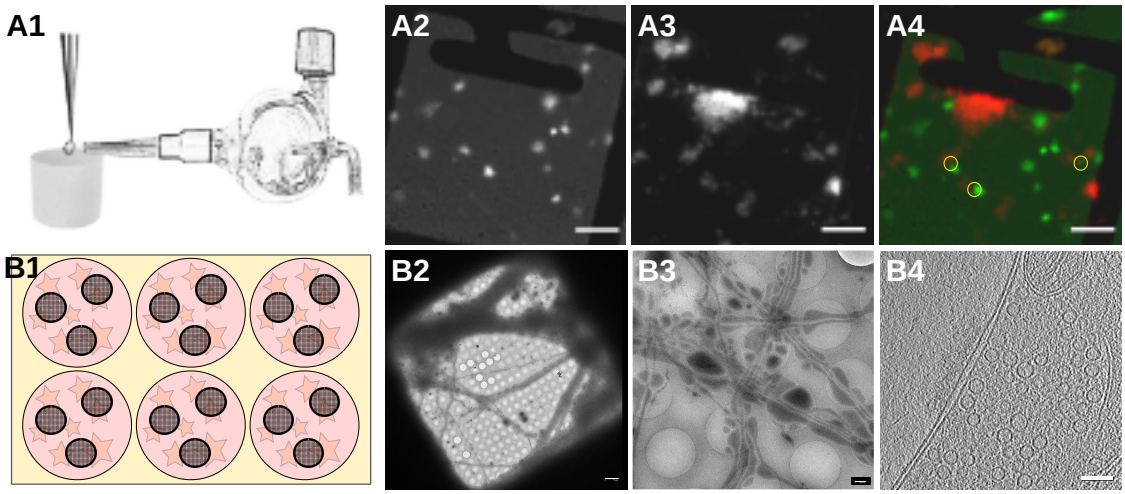

Figure 1: Experimental models. A1) Glass atomizer used to disperse depolarizing solution on the EM grid milliseconds before the grid is vitrified. A2) Spray droplets imaged with the GFP filter set. A3) Synaptosomes imaged with the DAPI filter set. A4) Overlay of spray droplets (green) and synaptosomes (red). Scale bars, 20 µm.

Increased membrane curvature at the onset of exocytosis

We analyzed the morphology of SVs fusing with the AZ PM. Synaptosomes of a single grid have not all been stimulated for the same duration. Some synaptosomes have been in contact with stimulating solution from the moment the droplet touched the grid, while some others were not at all in contact with the stimulating solution because no droplet landed close enough to them. Importantly, some synaptosomes were located near the point of impact of a droplet, in which case, it took some time for

KCl to diffuse until the concentration around these synaptosomes rose sufficiently to trigger exocytosis. Therefore, the time interval between triggering exocytosis and freezing ranged between 0 ms and the interval between spray droplets hitting the grid and freezing, which was comprised between 7 and 35 ms depending on the experiments (Table S2, see also [30]).

Synaptosomes from both control and sprayed grids were thoroughly analyzed for signs of exocytosis, which consisted of morphological changes of the AZ PM and the tethered SV occurring upon stimulation, which are described hereafter. These signs were only detected in synaptosomes from sprayed grids and are presented in the likeliest chronological order. Upon stimulation both the vesicle membrane and the PM were slightly bent towards each other (Figure ??B1, B2, and B3; orange arrows). These structures, which have previously been reported in liposomes but not in synapses, have been referred to as membrane curvature events [11]. Control synaptosomes (i.e. not sprayed) on the other hand, had a straight PM, and no SV membrane was buckled (Figure ??A). Following membrane bending we observed contacts between vesicles and the PM bilayer where both membranes lose their clear contours (Figure ??C1 & C2; pink arrows). This was followed by further transitioning states prior to and during pore opening (Figure ??D1, D2, and D3; blue arrows). In the next observed fusion state, the vesicle was wide open (Figure ??E), followed by almost completely collapsed vesicles where only a small bump on the PM remained visible (Figure ??F). These structures were not observed in any of the non-sprayed control datasets.

Stimulated synaptosome datasets were divided into early and late fusion stages, respectively, based on the morphology of SV and AZ PM. Synapses showing membrane bending and direct lipid contact between SV and PM without an open pore were classified as early fusion. Those with an open pore or a remaining small bump of a fully collapsed vesicle were classified as late fusion.

Synaptic vesicle distribution is impacted by synaptic activity

Non-stimulated rat synaptosomes as well as WT-SNAP-25 mouse cultured neuron synapses showed typical SV distribution, as observed in previous cryo-ET studies [13]. Vesicle occupancy was 0.08 in the most proximal zone (0-25 nm from the AZ PM), and peaked to 0.17 in 25-50 nm zone. It then dropped to 0.08 in the intermediate zone (50-75 nm) and rose steadily in the more distal zone to reach a plateau of ~0.16 from a distance of 125 nm (Figure ??). These values are for WT-SNAP-25 synapses. The absolute values differ between cultured mouse neurons and rat synaptosomes and but the SV occupancy distribution follows the very same pattern. The difference in absolute values can likely be attributed to the different experimental and animal models used. Sprayed synaptosomes that were showing early signs of exocytosis had a nearly identical SV occupancy pattern as non-sprayed synaptosomes. However, when SV full collapse figures were apparent, SV occupancy in the proximal zone was significantly reduced, whereas SV occupancy further away from the AZ PM was unchanged. This is consistent with some membrane proximal SVs having engaged in exocytosis while none of the recycling and reserve pool SVs have. In order to investigate the consequences of chronic high or low synaptic activity, we investigated the 4E and 4K mutants. In the proximal, intermediate, and the first distal areas (up to approximately 125 nm away from the AZ PM) SVs followed a similar occupancy pattern in the constitutively depressed 4E mutant. This confirmed that the lower activity of the 4E mutant was not due to a lack of SV availability. In the most distal zones, SV occupancy gradually decreased in the mutant *to become significantly different from a distance of XXX nm*. That latter decrease may reflect deleterious effects associated with abnormally low synaptic activity. The 4K mutant displayed significantly decreased SV occupancy in the most proximal area (up to 25 nm), which can be readily attributed to the high probability of spontaneous exocytosis generated by the additional positive charges of the SNARE bundle. From 25 nm to about 125 nm away from the AZ PM the occupancy pattern was similar to the WT situation. Beyond 125 nm occupancy dropped gradually and more steeply than in the case of the 4E mutant. *From a distance of XXX nm, occupancy was significantly lower than in the WT*. This decrease can also be explained by the high exocytosis rate, which leads to a depletion of the reserve pool.

RRP size evolution following stimulation

As stated in the Introduction, SVs that are linked by more than 2 tethers to the AZ PM have been shown to belong to the RRP. We investigated the tethering state of proximal SVs (i.e. those SVs within 45 nm of the AZ PM) prior and following stimulation in synaptosomes. In non-sprayed synaptosomes, 59% of the proximal vesicles were tethered, which is in agreement with previous results [13]. Interestingly, in the early fusion group the fraction of tethered proximal vesicles significantly increased to 80% ($P<0.05$, χ^2 test; Figure ??). In the late fusion group, however, 47% of the proximal vesicles were tethered, which is not significantly different to the non sprayed group. We then analyzed whether the decreased occupancy in the late fusion group was associated with a decreased number of RRP SVs. In resting, non-sprayed synapses about 11% of the proximal SVs resided in the RRP. This agrees with typical RRP size estimates based on electrophysiological measurements. Surprisingly, the fraction of proximal vesicles belonging to the RRP drastically increased to 36% in the early fusion group ($P<0.001$, χ^2 test; Figure ??). The fraction returned to the initial value of 11% in the late fusion group. This 3-fold increase over the baseline RRP SVs in the early fusion group suggests that upon stimulation some proximal SVs very rapidly enter the RRP and become primed for exocytosis. Furthermore, the lower proximal vesicle occupancy in the late fusion group indicates that under our stimulation conditions, replenishing vesicles to the proximal zone is slower than their release.

The situation in the WT-SNAP-25 neurons was similar to unstimulated synaptosomes. 53% of the all proximal SVs were tethered and 14% of all proximal SVs belonged to the RRP. WT proximal SVs The corresponding values for the 4E mutants were not significantly different. However, In all 4K mutant datasets there was not a single SV that was part of the RRP. Consistently, the number of tethers per proximal SV was significantly lower in the 4K mutant than in the WT. These results are in line with physiological measurements that have shown that the RRP is depleted in the chronically spontaneously active 4K mutant, and they provide additional evidence that RRP-vesicles have at least 3 tethers. [12].
Furthermore, the average distance between proximal SVs and the AZ PM is significantly higher in the 4K mutant than in the WT, suggesting that vesicles coming into close contact with the AZ PM undergo spontaneous exocytosis, and are depleted.

Synaptic activity modifies inter-SV connectivity

The majority of SV are connected to other SVs through so-called connectors [13,14]. Connector function and composition is not clear yet. It is generally assumed that synapsin is involved in connector formation and may be one of its components. It has been suggested that connectors reduce SV mobility and maintain a local high SV concentration in the presynpase. The connectivity level of an individual SV might be one of the factors defining the pool to which the SV belongs. To shed some light on the role of connectors we analyzed SV connectivity in our datasets. We focused most of *(all?)* our analysis to the SVs located at distance of the AZ PM lower than 250 nm. Furthermore, we defined 4 distance groups: proximal (0-45 nm), intermediate (45-75 nm), distal 1 (75-150 nm), distal 2 (150-250 nm), as in previous studies [13,31]. We first analyzed synaptosomes. In non-sprayed synaptosomes datasets, approximately 80% of the proximal and intermediate SVs were connected to other vesicles. In distal 1 and 2 regions, this value rose to 85 and 93%, respectively. sprayed, early and late fusion groups showed a similar pattern with one interesting exception. Proximal SV connectivity dropped to 58% in the late fusion group ($P<0.05$, χ^2 test; Figure [**figure:connectors?**]). This decrease originates from SVs that are not in the RRP of which only 52.9% of the vesicles were connected as opposed to 77.5% before stimulation ($P<0.01$, χ^2 test; Figure ??). These results are consistent with an observed decrease in the number of connectors per proximal SV that are not part of the RRP, from 1.81±0.18 connector per SV in the non sprayed group to 0.85±0.16 in the late fusion group ($P<0.01$, K-W test) (Figure ??). Connectors between proximal vesicles (Figure ??) were found to remain between fusing vesicles (Figure ?? and Supplementary movie S1). We hypothesize that given the free space made in the proximal region after some SVs have fused, non-connected vesicles from the

intermediate region diffuse to the proximal zone and become tethered to the AZ PM. Our data suggest that establishing connectivity is a slower process than tethering.

We then analyzed SNAP-25 mutants. Similarly to non-sprayed synaptosome, the fraction of connected SVs was significantly higher in the distal 2 group, albeit the absolute values were overall lower than in synaptosomes. SNAP-25-WT synapses showed a higher level of connectivity in the distal group. The fraction of connected SVs in both distal groups was significantly lower in the 4E mutant than in the WT. In the case of the 4K mutant, the difference was significant in the distal 2 group. Consistently, a significantly lower number of connectors per SV was observed in both distal groups of the 4E and the 4K mutants with respect to the WT. Additionally, the 4E mutant had significantly less connectors per proximal SV than the WT, whereas the 4K mutant had significantly less connectors per intermediate SV than the WT. These results indicate that prolonged abnormal exocytotic activity is correlated with changes in intervesicular connectivity.

Discussion

Materials and methods

Constructs and viruses

SNAP-25B was N-terminally fused to GFP and cloned into a pLenti construct with a CMV promoter [32]. Mutations were made using the QuikChange II XL kit (Agilent). The mutations were verified by sequencing and have been published before [12]. The preparation of lentiviral particles followed standard protocols.

Animals

Synaptosomes were prepared from adult male or female Wistar rat obtained from the central animal facilities of the Department of Biomedical Research of the University of Bern. Adult male or female Wistar rats at an age of 6-8 weeks were slightly stunned by CO2 and quickly decapitated with a guillotine. The procedures used were in accordance with the Swiss Veterinary Law guidelines. Heterozygous SNAP-25 KO C57/Bl6-mice were routinely backcrossed to Bl6 to generate new heterozygotes. The strain was kept in the heterozygous condition and timed heterozygous crosses and caesarean section were used to recover knockout embryos at embryonic day 18 (E18). Pregnant females were killed by cervical dislocation; embryos of either sex were collected and killed by decapitation. Permission to keep and breed SNAP-25 mice was obtained from the Danish Animal Experiments Inspectorate and followed institutional guidelines as overseen by the Institutional Animal Care and Use Committee (IACUC). CD1 outbred mice were used to create astrocytic cultures. Newborns (P0-P2) of either sex were used. Pups were killed by decapitation.

Synaptosome preparation

Rat synaptosomes were prepared as previously described [33], with some modifications. The cerebral cortex and the hippocampi were removed in sucrose buffer (SEH: 0.32 M sucrose, 1 mM EDTA, 10 mM HEPES; HEPES, #H4034, Sigma-Aldrich Corporate Offices. St. Louis, MO, USA) on ice. Homogenization of the tissue was done in SEH with a Potter-Elvehjem grinder (#358011, Wheaton. Millville, New Jersey, USA), four strokes at the bottom and 6 from top to bottom were applied to the tissue at a speed of 800 turns/min as described in [33]. The whole process from decapitation to homogenization was done within 2-3 min, to obtain functional synaptosomes. Homogenized tissue was then centrifuged at 1000 g for 10 min at 4°C to remove meninges and blood vessels. The resulting supernatant containing synaptosomes, but also gliosomes and mitochondria was then added to a discontinuous, isoosmotic

Percoll (#P1644, Sigma) gradient with 5%, 10% and 23% in 0.32 M sucrose, 1 mM EDTA in centrifuge tubes (#344060, Beckman Coulter). The samples were spun in an ultracentrifuge (rotor: SW 40 Ti; Beckman Coulter. Nyon, Switzerland) at 16400 rpm for 12 min at 4°C. The layer with the highest amount of functional synaptosomes was between 10-23 % [33]. The layer was carefully taken out and diluted 1:10 in HEPES buffered medium (HBM; 140 mM NaCl, 5 mM KCl, 5 mM $NaHCO_3$, 1.2 mM Na_2HPO_4, 1 mM $MgCl_2$, 10 mM Glucose, 20 mM HEPES). The obtained solution was further spun with an ultracentrifuge (rotor 45 Ti; Beckman Coulter) at 11200 rpm for 20 min at 4°C. The pellet was carefully and quickly aspirated with a Pasteur pipette to avoid mixture with the solution and then diluted in HBM.

Preparation of astrocytic and neuronal culture

The procedure has been published before [34]. Glial cells were ready to be used after 10 days. once they were triturated and counted with a Buerker chamber, 100,000 cells/ml were plated onto untreated 12 well plates containing 10% DMEM. Astrocytes were isolated from CD1 outbred mice (P0-P2). Pups were killed by decapitation and heads were placed in HBSS-HEPES medium (HBSS supplemented with 1 M HEPES). The cortices were isolated from the brains and the meninges were removed (dura, pia and arachnoid mater). The cortices were chopped into smaller fragments and transferred to a tube containing 0.25% trypsin dissolved in Dulbecco's MEM (DMEM)supplemented with 10% foetal calf serum, 20000 IU penicillin, 20 mg streptomycin and 1% MEM non-essential amino acids. Fragments were incubated for 15 min at 37°C. Subsequently, inactivation medium (12.5 mg albumin + 12.5 mg trypsin-inhibitor in 10% DMEM) was added and the tissue washed with HBSS-HEPES. Tissue was triturated until a smooth cloudy suspension appeared. Cells were plated in 80 cm^2 flasks with pre-warmed DMEM, one hemisphere per flask, and stored at 37°C with 5% CO_2. Glial cells were ready to be used after 10 days. Glial cells were washed with pre-warmed HBSS-HEPES. Trypsin was added and the flasks were incubated at 37°C for 10 min. Cells were triturated and counted with a Buerker chamber before plating 100,000 cells/ml on untreated 12-well plates containing DMEM. After 2 days, neurons were plated.

Hippocampal neurons were isolated from either E18 SNAP-25 KO. The SNAP-25 KO pups were obtained by pairing two heterozygote animals, and the embryos were recovered at E18 by caesarean section. Pups were selected based on the absence of motion after tactile stimulation and bloated neck [35]; the genotype was confirmed by PCR in all cases. The pups were killed by decapitation and heads were put in HBSS-HEPES medium. The cortices were isolated from the brains and the meninges were removed. The hippocampi were cut from the cortices before being transferred to a tube containing 0.25% trypsin dissolved in HBSS-HEPES solution. Fragments were incubated for 20 min at 37°C. Afterwards, the tissue was washed with HBSS-HEPES. The hippocampi were triturated and the cell count was determined with a Buerker chamber. 20 µl of solution containing 250,000 cells/ml were plated onto the flame sterilized gold R2/2 or R2/1 EM grids as previously described in [34]. Following a 30 min incubation at 37°C, the grid was transferred into the 12 well plate containing the astrocytes and medium was replaced with NB medium (Neurobasal with 2% B-27, 1 M HEPES, 0.26% lutamax, 14.3 mM β-mercaptoethanol, 20000 IU penicillin, 20 mg streptomycin) for the E18 pups or NB-A medium (Neurobasal-A with 2% B-27, 1% Glutamax , 20000 IU Penicillin, 20 mg Streptomycin) for the P0-P1. Between 4 h and 1 day later, lentiviral particles carrying either SNAP-25-WT, SNAP-25-4E, or SNAP-25-4K constructs were added to the culture. The cultures were incubated for 12 to 14 days before being plunge frozen.

Plunge freezing and spray-mixing

Rat synaptosomes were prepared for plunge freezing and spray-mixing as follows. The following steps from incubation to plunge freezing were all done at room temperature (RT), equivalent to 23-25°C. The synaptosomal solution was incubated with calcein blue AM (#C1429, Molecular Probes-Thermo Fisher Scientific. Waltham, MA, USA) 30 min prior to plunge freezing to visualize the cytosol of

functional – esterase containing – cellular compartments such as synaptosomes. Additionally, 1.3 mM CaCl2 and 10 nm gold fiducials were added (gold fiducials, #s10110/8. AURION Immuno Gold Reagents & Accessories. Wageningen, The Netherlands). CaCl2 is necessary to trigger exocytosis and gold fiducials are important to align the acquired tilt series for tomogram reconstruction. The sprayed solution contained 1 mM CaCl2 and 52 mM KCl in HBM to depolarize synaptosomes and trigger exocytosis. It also contained fluorescein (#46955, Sigma) to trace the spray droplets on the EM grid in cryo-FM. The synaptosomal solution was applied to a 200-mesh lacey finder carbon film grid (#AGS166-H2. Agar Scientific. Elektron Technology UK Ltd. Stansted, UK). Excess liquid on the grid was removed by blotting with a filter paper and the grid was immediately plunge frozen in liquid ethane with a homebuilt plunge freezer and was sprayed on the fly. The plunge freezer and the spraying device (atomizer) were computer controlled with a LabView script (National Instruments Corporation. Mopac Expwy Austin, TX, USA). The spraying device was set similarly to the device in [36]. Nitrogen gas pressure necessary to drive spraying was set to 2.5 bar. The grid was set to pass in front of the spray nozzle at a distance of 3-4 mm. The plunge freezer was accelerated to 0.75 m/s and the minimum spray delay was ~7 ms (Table S3). The atomizer sprays scattered droplets of various size on the EM grid. During the time lapse between spraying and freezing the content of the droplets spreads by diffusion. KCl diffuses approximately 4x faster than fluorescein. Cryo-ET imaging was done within the diffusion distance of KCl but outside of the visible spray droplet because the center of the spray droplet would usually be too thick for imaging. This reduces the effective stimulation duration to anything between 0 ms and less than the given spray-freeze delay. Moreover, through diffusion, KCl concentration rapidly rises and then decreases. Hence synaptosomes are not permanently depolarized.

After 12 to 14 days of incubation grids with mouse neurons were plunge frozen with a Vitrobot (Thermofisher Scientific, Mark IV) with a blot time of 3 s and a blot force of -10. Wait time and drain time were not used. Humidity was set to 100% at 4°C. 4 µl undiluted 10 nm BSA gold tracer (Aurion) was added directly onto the grid prior to plunge freezing.

Cryo-fluorescence microscopy

After plunge freezing, rat synaptsome samples were imaged at the fluorescent microscope under cryo conditions, with a Zeiss Axio Scope.A1, equipped with an AxioCam MRm camera (Carl Zeiss AG, Germany), and a fluorescence lamp (HXP 120 C). The correlative microscopy stage (#CMS196, Linkam Scientific Instruments, UK) was cooled down to -190°C by liquid nitrogen and the frozen EM grid was placed into the chamber of the cryostage on a bridge that was not submerged in liquid nitrogen and was close to the objective, where the temperature was around -150°C. The filter set used for imaging fluorescein was #38 (#000000-1031-346, Zeiss) (BP 470/40, FT 495, BP 525/50; corresponds to GFP) and the one for calcein blue AM was #49 (#488049-9901-000, Zeiss) (G 365, FT 395, BP 445/50; corresponds to DAPI). The objective used was either a 10x (#420941-9911, NA = 0.25 Ph1, Zeiss) or a 50x (#422472-9900, NA = 0.55 Dic, Zeiss), the acquisition software used was AxioVision (AxioVs40x64 V 4.8.3.0, Zeiss) and the processing software was ZEN lite (Zeiss).

Cryo-electron microscopy

Following cryo-FM, the rat synaptosome grids were mounted in a cryo-holder (Gatan, Pleasonton, CA, USA) and transferred to a Tecnai F20 (FEI, Eindhoven, The Netherlands) which was set to low dose conditions, operated at 200 kV, and equipped with a field emission gun. Images were recorded with a 2k x 2k CCD camera (Gatan) mounted after a GIF Tridiem post-column filter (Gatan) operated in zero-loss mode. The sample was kept at about -180°C. Tilt series were acquired using SerialEM [37] for automated acquisition recorded typically from -50° to 50° with a 2° angular increment and an unbinned pixel size of 0.75 or 1.2 nm. Due to sample thickness (400-700 nm), tomograms were usually not recorded with higher tilt angles. Defocus was set between -8 to -12 µm and the total electron dose used was about 80-100 $e^-/Å^2$. Some tomograms were acquired at a Titan Krios equipped with a K2

direct electron detector (Gatan) without energy filter. The K2 camera was operated in superresolution counting mode and between 8-40 frames per tilt angle were taken. Tilt series were acquired using the Latitude software (Gatan) for automated acquisition recorded typically from -60° to 60° with a 2° angular increment and an unbinned pixel size of 0.6 nm. Defocus was set between -8 to -12 µm and the total electron dose used was about 80-100 $e^-/Å^2$. Prior to image processing the frames at each tilt angle, frames were aligned and averaged in 2dx MC_Automator [38] with motioncor [39]. 3D reconstruction was done in IMOD [40]. The alignments were done using the automated fiducial tracking function and the 3D reconstructions were done using the weighted back projection followed by a nonlinear anisotropic diffusion (NAD) filtering. Following tomogram reconstruction only synaptosomes that fulfilled the following criteria were used: 1) even and non-broken PM, 2) synaptic cleft still attached to the presynapse, 3) spherical vesicles, and 4) a mitochondrion in the presynapse necessary to cover the energy demands of the synapse. These criteria indicate that the synaptosome is functional [41].

Cultured mouse neurons tilt series were acquired at a Titan Krios, equipped with a Falcon 3 direct electron detector (Thermofisher Scientific) without energy filter. The Falcon camera was operated in linear mode. Tilt series were acquired using the TEM Tomography software (TFS) for automated acquisition recorded typically from -60° to 60° with a 2° angular increment and an unbinned pixel size of 0.37 nm. Defocus was set between -6 to -10 µm and the total electron dose used was about 80-100 $e^-/Å^2$. Tomogram reconstruction was done as for synaptosome datasets.

Manual and automatic segmentation procedures

Manual segmentation of SVs, mitochondria, and the active zone PM was done in IMOD (Figure S4A&B). The boundary marked the region to be analyzed by Pyto [42]. The analysis by Pyto was essentially the same as described previously [13] [42]. In short, the segmented area is divided in 1 voxel thick layers parallel to the active zone for distance calculations. A hierarchical connectivity segmentation detects densities interconnecting vesicles (so called connectors) and densities connecting vesicles to the active zone PM (so called tethers) (Figure S4C). Distance calculations are done with the center of the vesicle. Mainly default settings were used. The segmentation procedure is conservative and tends to miss some tethers and connectors because of noise. Consequently, the numbers of tethers and connectors should not be considered as absolute values but rather to compare experimental groups. All tomograms analyzed by Pyto were obtained on the same microscope with the same tilt range. The margin of error for false negatives and positives was found to be less than 10% by comparison with ground truth [42]. As it was done before, an upper limit was set between 2100 and 3200 nm3 on segment volume. The tomograms that were used for this analysis were binned by a factor of 2 to 3, resulting in voxel sizes between 2.1 and 2.4 nm. Tether and connector length were calculated using the midpoint method [42]. From the stimulated synaptosomes only those that showed visible signs of exocytosis where used for analysis in Pyto.

Data analysis

If not stated otherwise data in the text are described as mean ± standard error to the mean (SEM). Wherever possible, data were presented as box plots with the following settings: orange bar, median; box extremities, lower and upper quartiles; whiskers extend up to 1.5 x interquartile range; dots, outliers. We used the same statistical tests as in [13,31]. For normal distributed data, the Student's t-test was used. ***remove the following sentence if necessary*** For data deviating from the normal distribution, the Kruskal-Wallis (K-W) test was used. In addition, for data that required to be split into discrete bins (e.g. fraction of connected vesicles by distance to active zone), the $\chi 2$ test was used. To calculate the correlation coefficient for paired samples (such as vesicle distance to active zone and number of tethers), Spearman's rank correlation was used (ρ-test). The confidence values were calculated using two-tailed tests and were indicated in the graphs by , *P<0.05;* , ***P<0.01;*** , P<0.001. We

did not apply statistical methods to predetermine sample size but similar sample sizes as previously reported have been used [13]. It was not necessary to apply randomization.

References

1. **Vesicle Docking in Regulated Exocytosis**
Matthijs Verhage, Jakob B Sørensen
Traffic (2008-09) https://doi.org/bjtx2n
DOI: 10.1111/j.1600-0854.2008.00759.x · PMID: 18445120

2. **Neurotransmitter Release: The Last Millisecond in the Life of a Synaptic Vesicle**
Thomas C Südhof
Neuron (2013-10) https://doi.org/f5gng4
DOI: 10.1016/j.neuron.2013.10.022 · PMID: 24183019 · PMCID: PMC3866025

3. **The readily releasable pool of synaptic vesicles**
Pascal S Kaeser, Wade G Regehr
Current Opinion in Neurobiology (2017-04) https://doi.org/gbkfsd
DOI: 10.1016/j.conb.2016.12.012 · PMID: 28103533 · PMCID: PMC5447466

4. **The Morphological and Molecular Nature of Synaptic Vesicle Priming at Presynaptic Active Zones**
Cordelia Imig, Sang-Won Min, Stefanie Krinner, Marife Arancillo, Christian Rosenmund, Thomas C Südhof, JeongSeop Rhee, Nils Brose, Benjamin H Cooper
Neuron (2014-10) https://doi.org/gcvj2v
DOI: 10.1016/j.neuron.2014.10.009 · PMID: 25374362

5. **The Synaptic Vesicle Release Machinery**
Josep Rizo, Junjie Xu
Annual Review of Biophysics (2015-06-22) https://doi.org/gjnb9q
DOI: 10.1146/annurev-biophys-060414-034057 · PMID: 26098518

6. **Crystal structure of a SNARE complex involved in synaptic exocytosis at 2.4 Å resolution**
RBryan Sutton, Dirk Fasshauer, Reinhard Jahn, Axel T Brunger
Nature (1998-09) https://doi.org/cwkm8k
DOI: 10.1038/26412 · PMID: 9759724

7. **Sequential N- to C-terminal SNARE complex assembly drives priming and fusion of secretory vesicles**
Jakob B Sørensen, Katrin Wiederhold, Emil M Müller, Ira Milosevic, Gábor Nagy, Bert L de Groot, Helmut Grubmüller, Dirk Fasshauer
The EMBO Journal (2006-02-23) https://doi.org/dhpwm3
DOI: 10.1038/sj.emboj.7601003 · PMID: 16498411 · PMCID: PMC1409717

8. **Single Vesicle Millisecond Fusion Kinetics Reveals Number of SNARE Complexes Optimal for Fast SNARE-mediated Membrane Fusion**
Marta K Domanska, Volker Kiessling, Alexander Stein, Dirk Fasshauer, Lukas K Tamm
Journal of Biological Chemistry (2009-11) https://doi.org/chdxqp
DOI: 10.1074/jbc.m109.047381 · PMID: 19759010 · PMCID: PMC2797286

9. **Fast Vesicle Fusion in Living Cells Requires at Least Three SNARE Complexes**
R Mohrmann, H de Wit, M Verhage, E Neher, JB Sorensen
Science (2010-09-16) https://doi.org/c7q87p
DOI: 10.1126/science.1193134 · PMID: 20847232

10. **SNARE Proteins: One to Fuse and Three to Keep the Nascent Fusion Pore Open**
L Shi, Q-T Shen, A Kiel, J Wang, H-W Wang, TJ Melia, JE Rothman, F Pincet

Science (2012-03-15) https://doi.org/gk8gpf
DOI: 10.1126/science.1214984 · PMID: 22422984 · PMCID: PMC3736847

11. **Membrane Curvature in Synaptic Vesicle Fusion and Beyond**
Harvey T McMahon, Michael M Kozlov, Sascha Martens
Cell (2010-03) https://doi.org/d3gmvv
DOI: 10.1016/j.cell.2010.02.017 · PMID: 20211126

12. **An Electrostatic Energy Barrier for SNARE-Dependent Spontaneous and Evoked Synaptic Transmission**
Marvin Ruiter, Anna Kádková, Andrea Scheutzow, Jörg Malsam, Thomas H Söllner, Jakob B Sørensen
Cell Reports (2019-02) https://doi.org/gfv5gd
DOI: 10.1016/j.celrep.2019.01.103 · PMID: 30811985

13. **Quantitative analysis of the native presynaptic cytomatrix by cryoelectron tomography**
Rubén Fernández-Busnadiego, Benoît Zuber, Ulrike Elisabeth Maurer, Marek Cyrklaff, Wolfgang Baumeister, Vladan Lučić
Journal of Cell Biology (2010-01-11) https://doi.org/b9c26b
DOI: 10.1083/jcb.200908082 · PMID: 20065095 · PMCID: PMC2812849

14. **Molecular architecture of the presynaptic terminal**
Benoît Zuber, Vladan Lučić
Current Opinion in Structural Biology (2019-02) https://doi.org/gk8gpd
DOI: 10.1016/j.sbi.2019.01.008 · PMID: 30925443

15. **Definition of the readily releasable pool of vesicles at hippocampal synapses.**
C Rosenmund, CF Stevens
Neuron (1996-06) https://www.ncbi.nlm.nih.gov/pubmed/8663996
DOI: 10.1016/s0896-6273(00)80146-4 · PMID: 8663996

16. **Properties of Synaptic Vesicle Pools in Mature Central Nerve Terminals**
Anthony C Ashton, Yuri A Ushkaryov
Journal of Biological Chemistry (2005-11) https://doi.org/cb5883
DOI: 10.1074/jbc.m504137200 · PMID: 16148008

17. **Vesicle release probability and pre-primed pool at glutamatergic synapses in area CA1 of the rat neonatal hippocampus**
Eric Hanse, Bengt Gustafsson
The Journal of Physiology (2001-03) https://doi.org/fq7th3
DOI: 10.1111/j.1469-7793.2001.0481i.x · PMID: 11230520 · PMCID: PMC2278469

18. **Reluctant Vesicles Contribute to the Total Readily Releasable Pool in Glutamatergic Hippocampal Neurons**
KL Moulder
Journal of Neuroscience (2005-04-13) https://doi.org/dwqpxj
DOI: 10.1523/jneurosci.5231-04.2005 · PMID: 15829636 · PMCID: PMC6724923

19. **Synaptic vesicle pools: an update**
Denker
Frontiers in Synaptic Neuroscience (2010) https://doi.org/d74dd7
DOI: 10.3389/fnsyn.2010.00135 · PMID: 21423521 · PMCID: PMC3059705

20. **The cytoskeletal architecture of the presynaptic terminal and molecular structure of synapsin 1.**
N Hirokawa, K Sobue, K Kanda, A Harada, H Yorifuji

Journal of Cell Biology (1989-01-01) https://doi.org/ddbqhb
DOI: 10.1083/jcb.108.1.111 · PMID: 2536030 · PMCID: PMC2115350

21. **Three-Dimensional Architecture of Presynaptic Terminal Cytomatrix**
L Siksou, P Rostaing, J-P Lechaire, T Boudier, T Ohtsuka, A Fejtova, H-T Kao, P Greengard, ED Gundelfinger, A Triller, S Marty
Journal of Neuroscience (2007-06-27) https://doi.org/bjw3mv
DOI: 10.1523/jneurosci.1773-07.2007 · PMID: 17596435 · PMCID: PMC6672225

22. **Physical determinants of vesicle mobility and supply at a central synapse**
Jason Seth Rothman, Laszlo Kocsis, Etienne Herzog, Zoltan Nusser, Robin Angus Silver
eLife (2016-08-19) https://doi.org/f9rmkt
DOI: 10.7554/elife.15133 · PMID: 27542193 · PMCID: PMC5025287

23. **Activity-Dependence of Synaptic Vesicle Dynamics**
Luca A Forte, Michael W Gramlich, Vitaly A Klyachko
The Journal of Neuroscience (2017-11-01) https://doi.org/gch7j3
DOI: 10.1523/jneurosci.0383-17.2017 · PMID: 28954868 · PMCID: PMC5666583

24. **Synapsin dispersion and reclustering during synaptic activity**
Ping Chi, Paul Greengard, Timothy A Ryan
Nature Neuroscience (2001-10-29) https://doi.org/cpdwc7
DOI: 10.1038/nn756 · PMID: 11685225

25. **Interactions of synapsin I with small synaptic vesicles: distinct sites in synapsin I bind to vesicle phospholipids and vesicle proteins.**
F Benfenati, M Bähler, R Jahn, P Greengard
Journal of Cell Biology (1989-05-01) https://doi.org/d65t4v
DOI: 10.1083/jcb.108.5.1863 · PMID: 2497106 · PMCID: PMC2115532

26. **Visualization of Synaptic Vesicle Movement in Intact Synaptic Boutons Using Fluorescence Fluctuation Spectroscopy**
Randolf Jordan, Edward A Lemke, Jurgen Klingauf
Biophysical Journal (2005-09) https://doi.org/cdpkkv
DOI: 10.1529/biophysj.105.061663 · PMID: 15980175 · PMCID: PMC1366711

27. **Synapsin Selectively Controls the Mobility of Resting Pool Vesicles at Hippocampal Terminals**
A Orenbuch, L Shalev, V Marra, I Sinai, Y Lavy, J Kahn, JJ Burden, K Staras, D Gitler
Journal of Neuroscience (2012-03-21) https://doi.org/f3wq83
DOI: 10.1523/jneurosci.5058-11.2012 · PMID: 22442064 · PMCID: PMC3492757

28. **High Mobility of Vesicles Supports Continuous Exocytosis at a Ribbon Synapse**
Matthew Holt, Anne Cooke, Andreas Neef, Leon Lagnado
Current Biology (2004-02) https://doi.org/b9g9h2
DOI: 10.1016/j.cub.2003.12.053 · PMID: 14761649

29. **Correlative microscopy: Bridging the gap between fluorescence light microscopy and cryo-electron tomography**
Anna Sartori, Rudolf Gatz, Florian Beck, Alexander Rigort, Wolfgang Baumeister, Juergen M Plitzko
Journal of Structural Biology (2007-11) https://doi.org/cp5krz
DOI: 10.1016/j.jsb.2007.07.011 · PMID: 17884579

30. **Analysis of transient structures by cryo-microscopy combined with rapid mixing of spray droplets.**

J Berriman, N Unwin
Ultramicroscopy (1994-12) https://www.ncbi.nlm.nih.gov/pubmed/7831735
DOI: 10.1016/0304-3991(94)90012-4 · PMID: 7831735

31. **Cryo–electron tomography reveals a critical role of RIM1α in synaptic vesicle tethering**
Rubén Fernández-Busnadiego, Shoh Asano, Ana-Maria Oprisoreanu, Eri Sakata, Michael Doengi, Zdravko Kochovski, Magdalena Zürner, Valentin Stein, Susanne Schoch, Wolfgang Baumeister, Vladan Lučić
Journal of Cell Biology (2013-05-27) https://doi.org/f4x2mj
DOI: 10.1083/jcb.201206063 · PMID: 23712261 · PMCID: PMC3664715

32. **Differential Abilities of SNAP-25 Homologs to Support Neuronal Function**
I Delgado-Martinez, RB Nehring, JB Sorensen
Journal of Neuroscience (2007-08-29) https://doi.org/d7mhxn
DOI: 10.1523/jneurosci.5092-06.2007 · PMID: 17728451 · PMCID: PMC6673127

33. **A rapid Percoll gradient procedure for preparation of synaptosomes**
Peter R Dunkley, Paula E Jarvie, Phillip J Robinson
Nature Protocols (2008-10-16) https://doi.org/b7zwh8
DOI: 10.1038/nprot.2008.171 · PMID: 18927557

34. **Preparation of Primary Neurons for Visualizing Neurites in a Frozen-hydrated State Using Cryo-Electron Tomography**
Sarah H Shahmoradian, Mauricio R Galiano, Chengbiao Wu, Shurui Chen, Matthew N Rasband, William C Mobley, Wah Chiu
Journal of Visualized Experiments (2014-02-12) https://doi.org/gmh9w3
DOI: 10.3791/50783 · PMID: 24561719 · PMCID: PMC4089403

35. **Genetic ablation of the t-SNARE SNAP-25 distinguishes mechanisms of neuroexocytosis**
Philip Washbourne, Peter M Thompson, Mario Carta, Edmar T Costa, James R Mathews, Guillermina Lopez-Benditó, Zoltán Molnár, Mark W Becher, CFernando Valenzuela, LDonald Partridge, Michael C Wilson
Nature Neuroscience (2001-12-19) https://doi.org/fbmxgc
DOI: 10.1038/nn783 · PMID: 11753414

36. **Analysis of transient structures by cryo-microscopy combined with rapid mixing of spray droplets**
John Berriman, Nigel Unwin
Ultramicroscopy (1994-12) https://doi.org/ctwp5j
DOI: 10.1016/0304-3991(94)90012-4

37. **Automated electron microscope tomography using robust prediction of specimen movements**
David N Mastronarde
Journal of Structural Biology (2005-10) https://doi.org/ff7gzx
DOI: 10.1016/j.jsb.2005.07.007 · PMID: 16182563

38. **2dx_automator: Implementation of a semiautomatic high-throughput high-resolution cryo-electron crystallography pipeline**
Sebastian Scherer, Julia Kowal, Mohamed Chami, Venkata Dandey, Marcel Arheit, Philippe Ringler, Henning Stahlberg
Journal of Structural Biology (2014-05) https://doi.org/f522h3
DOI: 10.1016/j.jsb.2014.03.016 · PMID: 24680783

39. **Electron counting and beam-induced motion correction enable near-atomic-resolution single-particle cryo-EM**
Xueming Li, Paul Mooney, Shawn Zheng, Christopher R Booth, Michael B Braunfeld, Sander Gubbens, David A Agard, Yifan Cheng
Nature Methods (2013-05-05) https://doi.org/f4zpjf
DOI: 10.1038/nmeth.2472 · PMID: 23644547 · PMCID: PMC3684049

40. **Computer Visualization of Three-Dimensional Image Data Using IMOD**
James R Kremer, David N Mastronarde, JRichard McIntosh
Journal of Structural Biology (1996-01) https://doi.org/d9nfzw
DOI: 10.1006/jsbi.1996.0013 · PMID: 8742726

41. **A rapid Percoll gradient procedure for isolation of synaptosomes directly from an S1 fraction: viability of subcellular fractions**
Steven M Harrison, Paula E Jarvie, Peter R Dunkley
Brain Research (1988-02) https://doi.org/b5tzcr
DOI: 10.1016/0006-8993(88)91384-4

42. **Hierarchical detection and analysis of macromolecular complexes in cryo-electron tomograms using Pyto software**
Vladan Lučić, Rubén Fernández-Busnadiego, Ulrike Laugks, Wolfgang Baumeister
Journal of Structural Biology (2016-12) https://doi.org/f9d5t2
DOI: 10.1016/j.jsb.2016.10.004 · PMID: 27742578